J. Fluid Mech. (2009), *vol.* 632, *pp.* 457–474.
doi:10.1017/S0022112009007484 Printed in the United Kingdom

A generalized Osborn–Cox relation

CARSTEN EDEN[1]†, DIRK OLBERS[2]
AND RICHARD J. GREATBATCH[1]

[1]Leibniz Institute of Marine Sciences at Kiel University, 24105 Kiel, Germany
[2]Alfred-Wegener-Institute for Polar and Marine Research, 27515 Bremerhaven, Germany

(Received 29 April 2008 and in revised form 12 March 2009)

The generalized temporal residual mean (TRM-G) framework is reviewed and illustrated using a numerical simulation of vertical shear instability. It is shown how TRM-G reveals the physically relevant amount of diapycnal eddy fluxes and implied diapycnal mixing, and how TRM-G relates to the Osborn–Cox relation, which is often used to obtain observational estimates of the diapycnal diffusivity. An exact expression for the diapycnal diffusivity in the TRM-G is given in the presence of molecular diffusion, based on acknowledging and summing up an entire hierarchy of eddy buoyancy moments. In this revised form of the Osborn–Cox relation, diapycnal diffusivity is related only to irreversible mixing of buoyancy, since all advective and molecular flux terms are converted to dissipation of variance and higher order moments. An approximate but closed analytical expression can be given for the revised Osborn–Cox relation with the caveat that this closed expression implies unphysical cross-boundary rotational fluxes.

It is demonstrated that the original Osborn–Cox relation, in which advective and molecular flux terms are simply neglected, is an approximation to the full form valid to first order. In the numerical simulation the original Osborn–Cox relation holds to a surprisingly good approximation despite large advective fluxes of variance and large lateral inhomogeneity in the turbulent mixing.

1. Introduction

The Osborn–Cox relation (Osborn & Cox 1972) considers a simplified eddy variance budget for a tracer and locally relates production of variance to molecular dissipation while neglecting advective and molecular fluxes of variance. Eddy variance denotes here (half of) the square of tracer perturbations given by deviations from Reynolds averaged quantities. The production of variance is part of the eddy tracer flux in the direction of the gradient of the mean tracer. Since that part of the eddy tracer flux can also be related to a turbulent diffusivity, the Osborn–Cox relation offers the possibility to relate the turbulent diffusivity to estimates of dissipation. Specifying buoyancy as the tracer under consideration, this diffusivity becomes the diapycnal diffusivity, which plays for instance an important role for the large-scale ocean circulation (Wunsch & Ferrari 2004). Therefore, considerable efforts have been made during the last years to obtain accurate observational estimate of the diapycnal diffusivity in the ocean (e.g. Schmitt *et al.* 2005).

† Email address for correspondence: ceden@ifm-geomar.de

The use of the Osborn–Cox relation to estimate the diapycnal diffusivity was criticised by Winters & D'Asaro (1995), stating that the average of the molecular flux across instantaneous isosurfaces of tracers (which they called the diascalar flux) is not necessarily identical to the turbulent (plus molecular) eddy flux across mean tracer isosurfaces (which they call the advective flux and which is used in the Osborn–Cox relation to determine the diffusivity). By defining a new coordinate which monotonically increases with instantaneous values of the tracer under consideration, they proposed a method to estimate the physically relevant eddy flux. The associated diffusivity is given by the molecular diffusivity enhanced by the ratio between the instantaneous area of tracer isosurfaces to the area of the mean tracer isosurface. The method of Winters & D'Asaro (1995) is akin to the effective diffusivity of Nakamura (1996) which was developed independently for the estimates of large-scale lateral mixing in the stratosphere. The use of a tracer coordinate replacing the vertical coordinate and its benefits for the interpretation of diapycnal eddy fluxes is also often discussed for application to large-scale ocean dynamics (De Szoeke & Bennett 1993; McDougall & McIntosh 2001).

However, the use of a tracer related coordinate to estimate diapycnal diffusivity is hampered by practical difficulties (Gregg 1998), since the method requires detailed knowledge of the instantaneous two-dimensional buoyancy surfaces, while observations are limited to one-dimensional vertical profiles of buoyancy. In practice, observationists often prefer to use the so-called method of 'Thorpe-sorting' (Thorpe 1977; Dillon & Park 1987) applied to observed profiles of tracer fluctuations, with results close to the method by Winters & D'Asaro (1995). On the other hand, the temporal residual mean (TRM) framework, pioneered by McDougall & McIntosh (1996) and discussed in general form by Eden, Greatbatch & Olbers (2007), offers an alternative theoretical approach to the method of Winters & D'Asaro (1995) based on a fixed, tracer independent coordinate system. The TRM (or TRM-G as the generalized form) is an extension of the transformed Eulerian mean (TEM) theory developed by Andrews & McIntyre (1976) for zonal mean flows and by Plumb (1990) and Plumb & Ferrari (2005) for three-dimensional quasi-geostrophic flows. In contrast to the original TEM theory by Andrews & McIntyre (1976), a part of the turbulent eddy flux is interpreted in TRM-G as a rotational flux which does not affect the mean tracer budget and should therefore not be related to a turbulent diffusivity. It was shown by Eden *et al.* (2007) that only the physically relevant cross-isopycnal eddy fluxes are associated with a turbulent diffusivity in the TRM-G.

Both the TEM and the TRM framework were originally developed for quasi-geostrophic (or synoptic) eddy activity in the atmosphere and the ocean. Since this dynamical regime is believed to involve only weak diapycnal mixing, applications and discussions of the TRM theory (McDougall & McIntosh 1996, 2001) have tended to focus on the lateral effects of mixing by quasi-geostrophic eddies, often interpreted as advection of buoyancy or mixing of potential vorticity, while diapycnal mixing has not been considered. Here, we review the TRM-G framework of Eden *et al.* (2007) and demonstrate, using a numerical simulation of vertical shear instability with large diapycnal mixing, that the TRM-G is also useful to interpret mixing in this dynamical regime. In fact, we are able to show that the Osborn–Cox relation still holds to first order in our experiment, i.e. better than one might have expected, given the presence of large advective fluxes of variance and strong inhomogeneities of the mean fields.

Similar to the method by Winters & D'Asaro (1995), practical complications due to higher order derivatives also hamper the application of the TRM-G for the analysis of in situ observations. On the other hand, the TRM-G turns out to be useful

for estimates of the turbulent diapycnal diffusivity in model simulations. In contrast to methods based on tracer dependent coordinates (Winters & D'Asaro 1995; Nakamura 1996), TRM-G yields a turbulent diffusivity localized in space rather than a bulk integral diffusivity as a function of the tracer dependent coordinate. The TRM-G estimate is also shown to be superior to a diffusivity estimated from a simple flux/gradient relationship. This is because the diffusivity in TRM-G is only related to irreversible mixing of the tracer under consideration, while the diffusivity estimated from the flux/gradient relationship can be strongly biased due to the presence of rotational eddy fluxes.

After describing the numerical simulation and the mean tracer distribution in the following section, we estimate the turbulent diffusivity in the simulation based on the total cross-isopycnal eddy fluxes within the TEM framework of Andrews & McIntyre (1976) in § 3 and discuss the estimate implied by the original Osborn–Cox relation in § 4. We find both estimates rather different and explain this difference by discussing rotational eddy fluxes following the TRM-G framework in § 5. In § 6, we furthermore account for the presence of rotational fluxes of variances and higher order moments following the TRM-G, which then ultimately leads to the generalized Osborn–Cox relation where all the advective and molecular flux terms are taken into account leaving only dissipative terms behind, which are used in turn to determine the diffusivity. We also discuss an approximate form of the TRM-G in § 7 which leads to a closed simplified form of the generalized Osborn–Cox relation. In § 8, we compare the different local estimates of mixing with the non-local estimate by Winters & D'Asaro (1995), while the last section summarizes and discusses the results.

2. Mean tracer equation and numerical model

We concentrate on the two-dimensional tracer equation

$$b_t + \boldsymbol{u}\cdot\nabla b = \nabla\cdot\kappa\nabla b, \tag{2.1}$$

where b denotes a tracer, $\boldsymbol{u}$ velocity with $\nabla\cdot\boldsymbol{u}=0$ and κ a molecular (or subgrid scale) diffusivity, which we take to be constant. We define a Reynolds average $\bar{()}$ for which the usual rules apply and which could be a time or ensemble mean. The (Reynolds) averaged tracer budget is then given by

$$\bar{b}_t + \bar{\boldsymbol{u}}\cdot\nabla\bar{b} = \nabla\cdot\kappa\nabla\bar{b} - \nabla\cdot\overline{\boldsymbol{u}'b'}, \tag{2.2}$$

where $b'=b-\bar{b}$ and $\boldsymbol{u}'=\boldsymbol{u}-\bar{\boldsymbol{u}}$ denotes tracer and velocity fluctuations, respectively. For illustration of the discussion we present results from a simulation of vertical shear instability in a two-dimensional channel (in x and z direction) using a non-hydrostatic numerical model (The numerical code together with all configurations used in this study can be accessed at http://www.ifm-geomar.de/~cpflame.). Note, however, that all analytical results discussed here carry over to the three-dimensional case.

Figure 1 shows a snapshot in terms of buoyancy and velocity from the simulation. Large vertical shear and uniform vertical stratification are prescribed by linear relaxation of buoyancy and velocity in a restoring zone over the whole depth range from $x=0\,\mathrm{m}$ to $x=2\,\mathrm{m}$ in a channel of 60 m length (see figure 1) with a time scale of 0.2 s (note that the restoring zone is just to the left of the region shown in figure 1). The prescribed velocity within the restoring zone is $\boldsymbol{u}=(1,0)\,\mathrm{m\,s^{-1}}$ for $z>-8\,\mathrm{m}$ and $\boldsymbol{u}=(3,0)\,\mathrm{m\,s^{-1}}$ for $z<-8\,\mathrm{m}$ and the prescribed constant vertical buoyancy gradient within the restoring zone is $\frac{\partial}{\partial z}\bar{b}=N_0^2$ with $N_0=0.02\,\mathrm{s^{-1}}$. Outside the restoring zone the flow is free to evolve. The vertical boundary conditions are free slip for momentum and zero flux of buoyancy. The channel is periodic in the x direction, with the effect

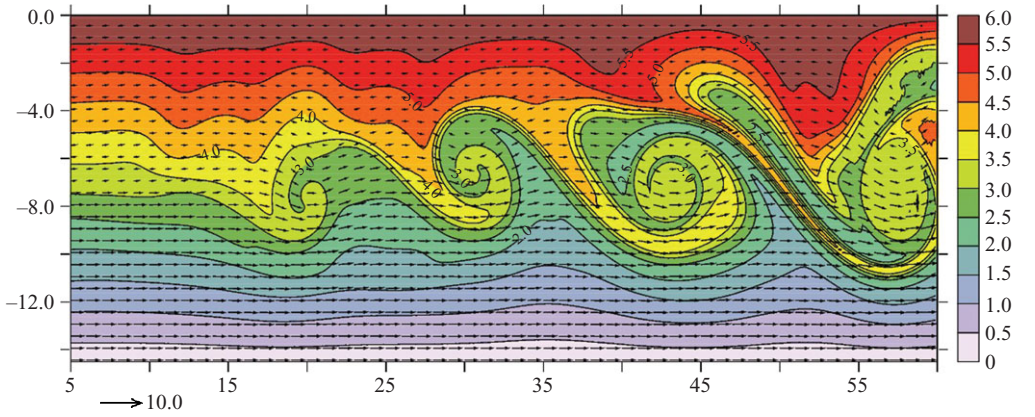

FIGURE 1. Snapshot of buoyancy (in $10^{-3}\,\mathrm{m\,s^{-2}}$) and velocity (arrows) in a simulation of vertical shear instability. The vector shown below the figure corresponds to $10\,\mathrm{m\,s^{-1}}$.

that the large perturbations seen in figure 1 propagating into the restoring zone are strongly damped and serve as small initial perturbations when propagating out of the restoring zone on the left side of figure 1.

Horizontal and vertical resolution of the model domain is 0.125 m and the time step is 1.25×10^{-2} s. The subgrid-scale horizontal and vertical harmonic diffusivity and viscosity is $\kappa = 5 \times 10^{-3}\ \mathrm{m^2\,s^{-1}}$. The magnitude of diffusivity and viscosity was chosen in order to limit vertical grid Péclet and Reynolds numbers to less than approximately 10 in the intense mixing zones. A prognostic equation for buoyancy is solved in the model subject to harmonic diffusion (and the restoring zone), while there is no implicit numerical diffusion (we use a fourth-order centred difference advection scheme). The flow is in quasi-stationary equilibrium after a couple of minutes and the results are taken from a 1 h period of model time after the initial spin-up.

3. Diapycnal eddy fluxes

The large vertical shear in the channel which is prescribed in the restoring zone at $x < 5$ m, leads to rapidly growing Kelvin–Helmholtz instabilities and to a large lateral inhomogeneity. Strong eddy activity downstream of the restoring zone can be seen in the snapshot shown in figure 1. The familiar Kelvin–Helmholtz billows, characteristic of vertical shear instability, show up in the simulation such that we can expect strong mixing of buoyancy. The eddy activity leads indeed to an eddy flux across contours of mean buoyancy (figure 2), i.e. to a cross-isopycnal eddy flux. It is predominantly upwards (down gradient) but there is also a (isopycnal) component along contours of the mean buoyancy. Contours of mean buoyancy (figure 2) are diverging downstream of the restoring zone indicating also diapycnal mixing of $\bar{b}$ by the eddy activity. It is therefore tempting to relate the cross-isopycnal eddy flux to the mixing of the mean buoyancy.

To diagnose the mixing of mean buoyancy we first follow the TEM framework of Andrews & McIntyre (1978) in which the eddy flux is decomposed into a component across and a (isopycnal) component along contours of the mean buoyancy, i.e

$$\overline{\boldsymbol{u}'b'} = -K_{TEM}\nabla\bar{b} + B_{TEM}\underline{\nabla}\bar{b}, \tag{3.1}$$

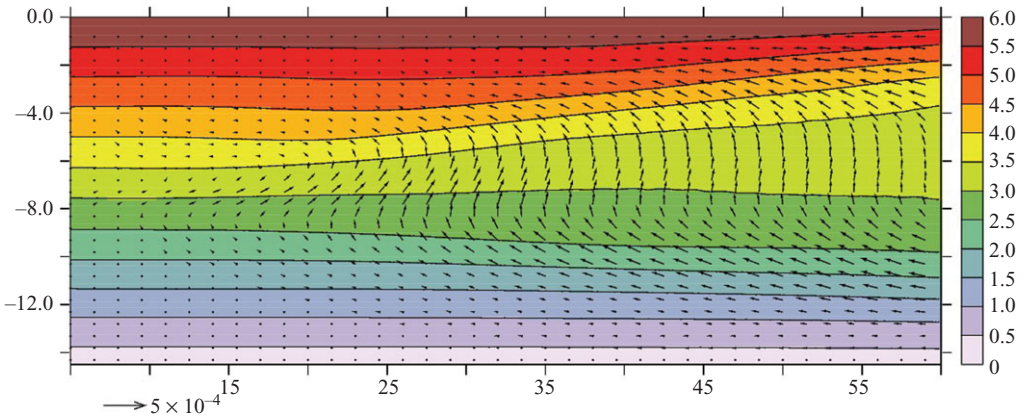

FIGURE 2. Mean buoyancy $\bar{b}$ (in $10^{-3}\,\mathrm{m\,s^{-2}}$) and eddy buoyancy flux $\overline{\boldsymbol{u}'b'}$. The flux vector was box averaged (12 points in x and 4 points in z direction). The vector shown below the figure corresponds to $5 \times 10^{-4}\,\mathrm{m^2\,s^{-3}}$.

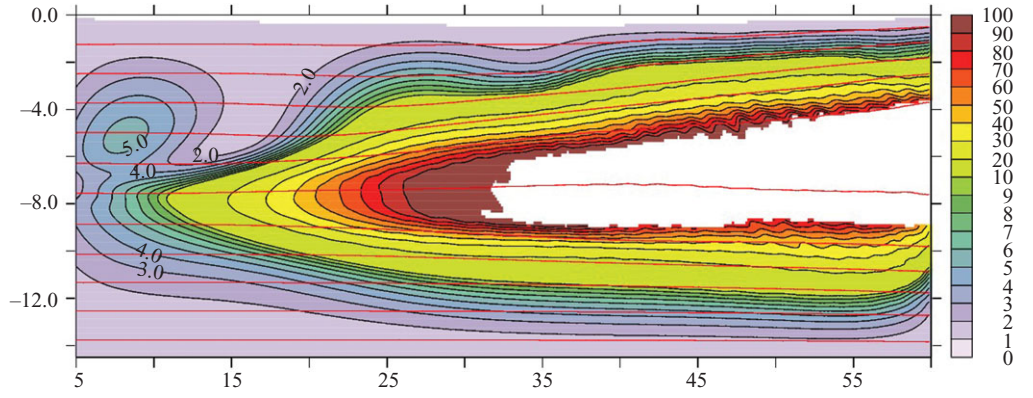

FIGURE 3. TEM-based estimate of the effective diffusivity relative to the subgrid-scale diffusivity in the form $(K_{TEM} + \kappa)/\kappa$. Regions in which $|\nabla\bar{b}|^{1/2} < 0.015\ \mathrm{s^{-1}}$ are not shaded. Also shown are contours of the mean buoyancy (red lines).

introducing the curl operator $\underset{\neg}{\nabla} = (-\frac{\partial}{\partial z}, \frac{\partial}{\partial x})$. Using the expression in the mean buoyancy budget (defined in (2.2)), $K_{TEM} = -|\nabla\bar{b}|^{-2}\overline{\boldsymbol{u}'b'} \cdot \nabla\bar{b}$ is identified as a turbulent diapycnal diffusivity, while B_{TEM} acts as a streamfunction of eddy driven flow. Note that the latter plays the dominant role for quasi-geostrophic eddy activity in the atmosphere and the ocean and also in the theory of Andrews & McIntyre (1978) while the diapycnal diffusivity K_{TEM} is often neglected since it is considered to be small. In contrast, however, we will concentrate here on the diapycnal diffusivity, and we will not further discuss the streamfunction B_{TEM}.

K_{TEM} was diagnosed in the numerical simulation and is shown relative to the subgrid-scale diffusivity κ in figure 3. Since K_{TEM} gets very large and its estimate uncertain (because of finite differencing and to a smaller extent by temporal averaging) when the gradient of the mean buoyancy gets low, which is the case in the well-mixed region downstream of the source region for $x \gtrsim 30\,\mathrm{m}$, we show K_{TEM} for regions in which $|\nabla\bar{b}|^{1/2} > 0.015\,\mathrm{s^{-1}}$ only, corresponding to regions where the ratio between the threshold value for $|\nabla b|$ and the stratification of the unperturbed (background) state

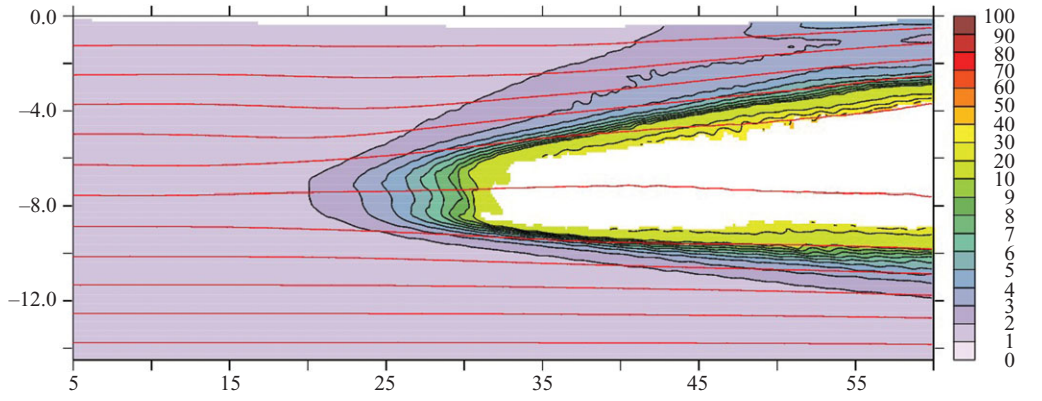

FIGURE 4. $1+\bar{C}$ in the numerical simulation, where $\bar{C}$ denotes the Cox number. Regions in which $|\nabla\bar{b}|^{1/2} < 0.015\,\mathrm{s}^{-1}$ are not shaded. Also shown are contours of the mean buoyancy (red lines).

exceeds 1/2. It is obvious that the increasing eddy activity downstream of the source region leads to a diapycnal turbulent diffusivity K_{TEM} which is more than 100 times larger than the subgrid-scale diffusivity κ. However, we argue here that much of the eddy activity is related to a rotational eddy flux without any local mixing effect due to a divergence of the eddy flux. We stress that such a rotational eddy flux should not be associated with a diffusivity. We show below that this rotational eddy flux is associated with an advective flux of variance along mean isopycnals which is rather large in the numerical simulation.

4. Original Osborn–Cox relation

A physical interpretation of the turbulent diapycnal diffusivity is offered by the Osborn–Cox relation, based on the budget of buoyancy variance given by

$$(\overline{\phi_2})_t + \nabla\cdot(\overline{\boldsymbol{u}\phi_2} - \kappa\nabla\overline{\phi_2}) = -\kappa\overline{|\nabla b'|^2} - \overline{\boldsymbol{u}'b'}\cdot\nabla\bar{b}, \tag{4.1}$$

where $\phi_2 = b'^2/2$. Neglecting in the steady variance budget (i.e. for $(\overline{\phi_2})_t = 0$) for a moment the advective and molecular fluxes we obtain a local relation between production $(\overline{\boldsymbol{u}'b'}\cdot\nabla\bar{b})$ and dissipation of variance $(\kappa\overline{|\nabla b'|^2})$ by molecular diffusion. Using the TEM decomposition for the eddy buoyancy flux (defined in (3.1)), the Osborn–Cox relation is recovered

$$K_{TEM} = \kappa\bar{C}, \tag{4.2}$$

where $\bar{C} = \frac{\overline{|\nabla b'|^2}}{|\nabla\bar{b}|^2}$ is sometimes called the Cox number. It measures the relation between squared gradients of perturbation to the squared gradients of the mean tracer and its knowledge allows calculation of the turbulent diffusivity. For turbulent flows it is normally found that $\bar{C} \gg 1$, such that the Osborn–Cox relation demonstrates how the turbulence enhances the effect of molecular diffusivity by increasing the instantaneous gradients relative to the gradients of the mean buoyancy.

The Cox number in our simulation is shown in figure 4 on the same colour scale as the turbulent diffusivity K_{TEM} relative to the subgrid-scale diffusivity κ in figure 3. Although the lateral structure of $\bar{C}$ is similar to K_{TEM}/κ, it is in general smaller than K_{TEM}/κ implying much less mixing than the previous estimate. It is clear that this difference originates from the neglected advective variance fluxes (molecular variance

fluxes are much smaller) in the variance budget (defined in (4.1)), such that the validity of the Osborn–Cox relation and the implied diffusivity is not obvious. However, it is possible to eliminate the advective fluxes in the variance budget in a physically consistent way and to come to a more precise physical interpretation of the turbulent diffusivity as shown next.

5. Rotational eddy fluxes

Following the TRM-G framework of Eden *et al.* (2007), we decompose the eddy fluxes into their isopycnal and cross-isopycnal components, as before in the TEM decomposition, but in addition we now also account for rotational eddy fluxes. We also decompose the advective plus molecular fluxes in the variance budget in the same way, i.e.

$$\overline{\boldsymbol{u}'b'} = \underset{\neg}{\nabla}\theta_1 + B_1\underset{\neg}{\nabla}\bar{b} - K_1\nabla\bar{b} \quad , \quad \overline{\boldsymbol{u}\phi_2} - \kappa\nabla\overline{\phi_2} = \underset{\neg}{\nabla}\theta_2 + B_2\underset{\neg}{\nabla}\bar{b} - K_2\nabla\bar{b}, \tag{5.1}$$

Note that the rotational flux component $\underset{\neg}{\nabla}\theta_1$ drops out taking the divergence of the eddy flux $\overline{\boldsymbol{u}'b'}$ in the mean tracer budget (defined in (2.2)), such that, with respect to the mean budget, we are free to choose θ_1. The same holds for $\underset{\neg}{\nabla}\theta_2$ (which we have introduced for later use) and the divergence of the advective and molecular variance fluxes $\overline{\boldsymbol{u}\phi_2} - \kappa\nabla\overline{\phi_2}$ in the variance budget. θ_1 acts as a streamfunction for a rotational eddy buoyancy flux and will show up in the variance budget, a fact which will be used to understand and to obtain its value. K_1 takes the same meaning as K_{TEM} and acts as a turbulent diapycnal diffusivity in the mean tracer budget, while B_1 acts as a streamfunction of eddy-driven velocity. We get after some manipulations in the steady state variance budget

$$(\underset{\neg}{\nabla}\theta_1 - \underset{\neg}{\nabla}B_2)\cdot\nabla\bar{b} = -\kappa\overline{|\nabla b'|^2} + K_1|\nabla\bar{b}|^2 + \nabla\cdot K_2\nabla\bar{b}. \tag{5.2}$$

Now it is possible to choose $\theta_1 = B_2$ such that the advective terms vanish. In this setting, the rotational flux potential is given by the flux of variance circulating along contours of mean buoyancy. The 'localized' variance budget can then be solved for the turbulent diffusivity in steady state resembling a revised Osborn–Cox relation:

$$K_1 = \kappa\overline{C} - \mathscr{D}(K_2), \tag{5.3}$$

with the operator $\mathscr{D}() = |\nabla\bar{b}|^{-2}\nabla\cdot()\nabla\bar{b}$. It follows that K_1 can be generated in steady state either by dissipation of variance and/or a cross-isopycnal flux of variance, as noted first by Medvedev & Greatbatch (2004). Neglecting for a moment the diapycnal flux of variance related to K_2, the Osborn–Cox relation is recovered, i.e. a local balance between production and dissipation of variance.

Figure 5 shows $\overline{\boldsymbol{u}\phi_2}$ and its isopycnal component (B_2) in the numerical simulation. Note that we have set $\theta_2 = 0$ for the moment such that we show $B_2 = |\nabla\bar{b}|^{-2}\overline{\boldsymbol{u}\phi_2}\cdot\underset{\neg}{\nabla}\bar{b}$ in figure 5. We stress that $\theta_2 = 0$ is only used momentarily for the purpose of demonstration since this assumption will be dropped when we consider rotational fluxes of variance in the next section. The mean advection $\bar{\boldsymbol{u}}\overline{\phi_2}$ dominates in the total advective flux of variance $\overline{\boldsymbol{u}\phi_2} = \bar{\boldsymbol{u}}\overline{\phi_2} + \overline{\boldsymbol{u}'\phi_2}$ and the molecular flux is much smaller than the advective flux. Thus, the advective flux of variance is predominantly horizontal and positive in the x direction while its vertical component remains small.

Figure 6 shows the eddy buoyancy variance $\bar{\phi}_2$. It is increasing downstream of the source region due to the increasing eddy activity such that the advective flux of variance also increases with x. The result is that $B_2 = \theta_1$ shows a similar lateral

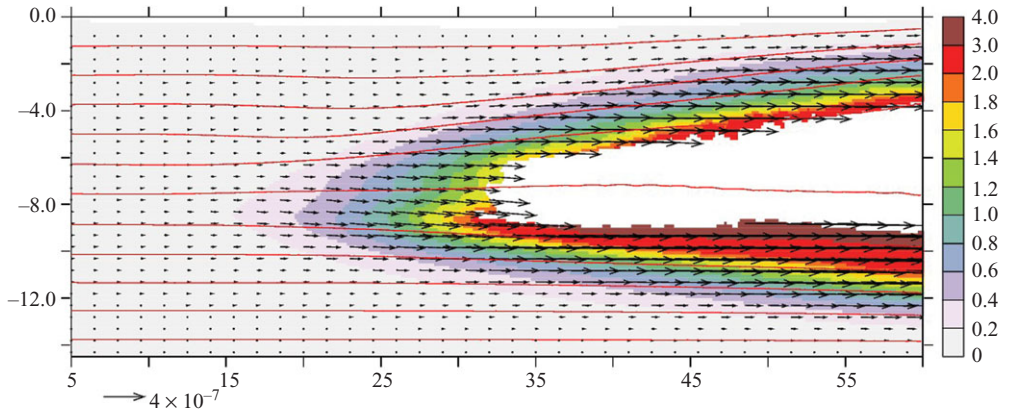

FIGURE 5. The advective flux of variance $\overline{\boldsymbol{u}\phi_2}$ (arrows) and its isopycnal component B_2 in $10^{-3}\,\mathrm{m^3\,s^{-3}}$ (shaded). B_2 was calculated setting $\theta_2 = 0$. The variance flux vector was box averaged (12 points in x and 4 points in z direction). The vector shown below the figure corresponds to $4 \times 10^{-7}\,\mathrm{m^3\,s^{-5}}$. Regions in which $|\nabla\bar{b}|^{1/2} < 0.015\,\mathrm{s^{-1}}$ are not shaded. Also shown are contours of the mean buoyancy (red lines).

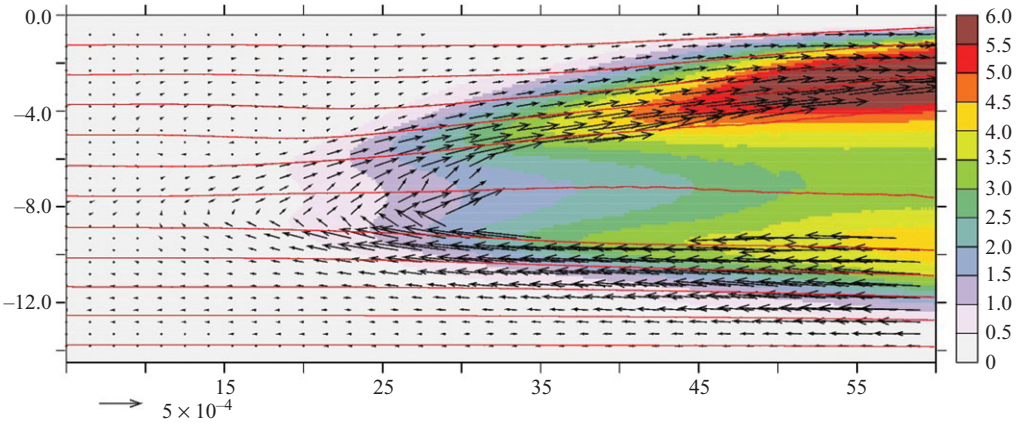

FIGURE 6. Buoyancy variance $\bar{\phi}_2$ in $10^{-6}\,\mathrm{m^2\,s^{-4}}$ (shaded) and rotational eddy flux (arrows) which was also box averaged (12 points in x and 4 points in z direction). The vector shown below the figure corresponds to to $5 \times 10^{-4}\,\mathrm{m^2\,s^{-3}}$. Regions in which $|\nabla\bar{b}|^{1/2} < 0.015\,\mathrm{s^{-1}}$ are not shaded. Also shown are contours of the mean buoyancy (red lines).

structure as the variance itself. The gauge potential θ_1 serves as a streamfunction for the rotational eddy flux $\overline{\nabla\theta_1}$ which is also shown in figure 6. Comparing the vertical rotational eddy flux $\overline{\nabla\theta_1}$ with the 'total' eddy flux $\overline{\boldsymbol{u}'b'}$ in figure 2 (note that the arrow scale is identical in both figures) it becomes obvious that a large part of the 'total' vertical eddy flux is in fact given by the rotational flux $\overline{\nabla\theta_1}$. In particular in the region $15\,\mathrm{m} \lesssim x \lesssim 30\,\mathrm{m}$ the vertical 'total' eddy flux of positive sign is almost completely made by the rotational eddy flux $\overline{\nabla\theta_1}$. This rotational component of the eddy flux is responsible for the large diapycnal diffusivities in figure 3 compared to the estimate using the original Osborn–Cox relation (4.2) and is related to the large advective fluxes of variance along isopycnals. Note that the flux of variance was neglected in

the original Osborn–Cox relation (4.2) and that only its cross-isopycnal component is related to a diapycnal diffusivity in the revised Osborn–Cox relation (5.3).

When the flow reaches the restoring zone (not shown in figure 6), the variance rapidly decays, such that the isopycnal flux of variance also vanishes. That means that the streamfunction θ_1 for the rotational eddy flux recirculates within the restoring zone. Note that there is no rotational eddy flux across the upper or lower boundary in this configuration.

6. Rotational variance fluxes

Comparing figure 6 and figure 2 it becomes obvious that the rotational eddy flux $\nabla\theta_1$ overcompensates the 'total' eddy flux $\overline{\boldsymbol{u}'b'}$ such that the resulting diffusivity, $\overrightarrow{K}_1 = |\nabla\bar{b}|^{-2}(\overline{\boldsymbol{u}'b'} - \nabla\theta_1)$, can get negative in some regions (not shown). This artifact is in fact related to a rotational flux component carried by the flux of variance, which we have already implicitly indicated by the definition of θ_2. Note that we have assumed $\theta_2 = 0$ in figures 5 and 6. Note also that another effect of the rotational flux of variance on the turbulent diffusivity is given by its cross-isopycnal component showing up in the revised Osborn–Cox relation (5.3). We will show below that the diapycnal component of the variance flux also shows a large rotational component, obscuring the revised Osborn–Cox relation (5.3).

We also note that the physical interpretation of the turbulent diffusivity in the revised Osborn–Cox relation (5.3) is hampered by the presence of the cross-isopycnal flux of variance. In consequence, the validity of the original Osborn–Cox relation (4.2) in which the cross-isopycnal flux of variance was neglected remains unclear. The meaning of the term is not obvious from the discussion so far, but it can also be related to dissipation of buoyancy moments when considering the rotational variance flux using the method of Eden *et al.* (2007).

Analogous to the gauge potential of the eddy buoyancy flux θ_1, for which the setting was obtained from the second buoyancy moment (variance) budget, we can obtain a setting for θ_2 from the budget of the third buoyancy moment. As outlined by Eden *et al.* (2007), it is in fact useful to consider the full hierarchy of centred buoyancy moments given by

$$(\overline{\phi_{n+1}})_t + n\bar{\phi}_n\bar{b}_t + \nabla\cdot\boldsymbol{f}_{n+1} = -\kappa n\nabla\overline{\phi_n}\cdot\nabla\bar{b} - \kappa n(n-1)\overline{\phi_{n-1}|\nabla b'|^2} - n\overline{\phi_n\boldsymbol{u}}\cdot\nabla\bar{b}, \quad (6.1)$$

with $\phi_n = \frac{b'^n}{n}$. All advective and molecular fluxes in the budget for $\overline{\phi_n}$ are combined in the flux vector $\boldsymbol{f}_n$, which is decomposed in turn as before into isopycnal and diapycnal components plus rotational fluxes, i.e.

$$\boldsymbol{f}_n = \overline{\boldsymbol{u}\phi_n} - \kappa\nabla\overline{\phi_n} - \kappa(n-1)\overline{\phi_{n-1}}\nabla\bar{b} = \underrightarrow{\nabla\theta_n} + B_n\underrightarrow{\nabla\bar{b}} - K_n\nabla\bar{b}. \quad (6.2)$$

Note that for buoyancy moments $n > 2$, two parts of molecular fluxes show up in $\boldsymbol{f}_n$ (both are small compared to the advective flux in the numerical simulation). However, all advective and molecular fluxes can be eliminated from all budgets of buoyancy moments by the choice $n\theta_n = B_{n+1}$ (analogous to (5.2)). We get after some manipulations for the steady budgets of the buoyancy moments

$$K_1 = \kappa\overline{C} - \mathscr{D}(K_2), \quad K_n = \kappa(n-1)\overline{\phi_{n-1}(1+C)} - \frac{1}{n}\mathscr{D}(K_{n+1}) + 2\kappa\mathscr{F}(\bar{\phi}_n), \quad (6.3)$$

with the operator $\mathscr{F}() = |\nabla\bar{b}|^{-2}\nabla\bar{b}\cdot\nabla()$. Solving now subsequently for the turbulent diapycnal diffusivity K_1 we obtain the following generalized form of the Osborn–Cox

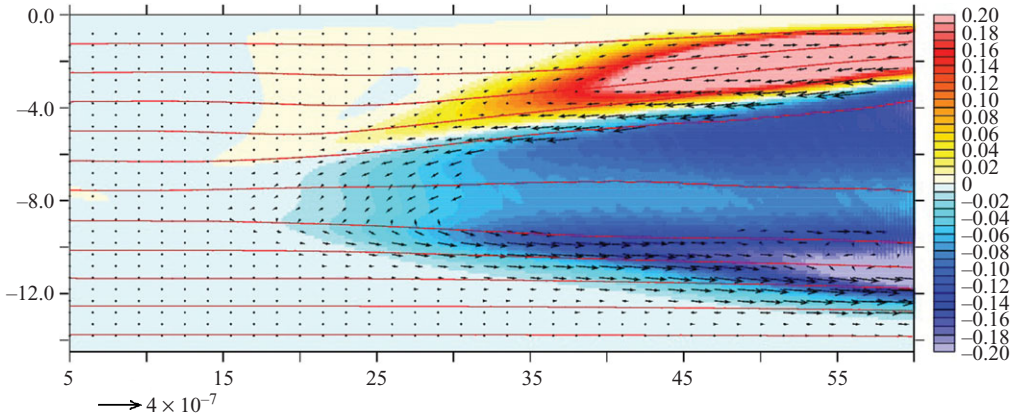

FIGURE 7. Buoyancy skewness $\bar{\phi}_3$ in $10^{-9}\,\mathrm{m^3\,s^{-6}}$ (shaded) and rotational flux of variance (arrows). B_3 was estimated setting θ_3 to zero. The flux vector was box averaged (12 points in x and 4 points in z direction). The vector shown below the figure corresponds to $4\times10^{-7}\,\mathrm{m^3\,s^{-5}}$. Regions in which $|\nabla\bar{b}|^{1/2}<0.015\,\mathrm{s^{-1}}$ are not shaded. Also shown are contours of the mean buoyancy (red lines).

relation

$$K_1+\kappa=\kappa\left[(1+\overline{C})-\mathscr{D}\overline{\phi_1(1+C)}+\mathscr{D}^2\overline{\phi_2(1+C)}-\frac{1}{2}\mathscr{D}^3\overline{\phi_3(1+C)}\right.$$
$$\left.+\frac{1}{3!}\mathscr{D}^4\overline{\phi_4(1+C)}-\cdots-2\mathscr{D}\mathscr{F}\bar{\phi}_2+2\frac{1}{2}\mathscr{D}^2\mathscr{F}\bar{\phi}_3-2\frac{1}{3!}\mathscr{D}^3\mathscr{F}\bar{\phi}_4+\cdots\right]. \quad (6.4)$$

In contrast to the original Osborn–Cox relation (4.2), the generalized form (6.4) of the variance budget is exact for steady flow (compare Eden *et al.* 2007 for the generalized Osborn–Cox relation including growth and decay of buoyancy moments). In contrast to the revised form given by (5.3), the diapycnal flux of variance which we found hard to interpret, has been converted to dissipative terms which are all proportional to the subgrid-scale diffusivity κ. The term has now a clear physical meaning: Turbulent diffusivity K_1 is locally related to dissipation of buoyancy moments in subsequent order. K_1 is zero if there is no subgrid-scale mixing.

From the setting $n\theta_n=B_{n+1}$ we can estimate now the rotational flux of variance $\theta_2=\frac{1}{2}B_3$ where B_3 denotes the isopycnal component of the flux of the third buoyancy moment, $\overline{\boldsymbol{u}\phi_3}$. Figure 7 shows the buoyancy skewness $\bar{\phi}_3$ in the numerical simulation. It is negative over large regions, only in the upper layer ϕ_3 gets positive. Also shown is the rotational flux of variance $\overline{\nabla}\frac{1}{2}B_3$. The rotational flux of ϕ_3 given by $\overline{\nabla}\theta_3$ was set momentarily to zero in order to diagnose B_3 (it is given by $\theta_3=\frac{1}{3}B_4$ in TRM-G).

In the lower half of the channel, the rotational variance flux is horizontal and positive in the x direction, i.e. contributing to a large portion of the 'total' flux of variance, $\overline{\boldsymbol{u}\phi_2}$ as shown in figure 5 (using identical vector length in both figures). In the upper part of the channel $\overline{\nabla}\frac{1}{2}B_3$ is horizontal and negative in x direction, i.e. of opposite sign of the 'total' variance flux. The overcompensation of the 'total' eddy flux $\overline{\boldsymbol{u}'b'}$ by the rotational flux, as observed when setting $\theta_2=0$, is reduced but not completely eliminated. Note that the rotational component of the flux of skewness given by θ_3 (not shown) will give a further correction to the rotational eddy flux and so on.

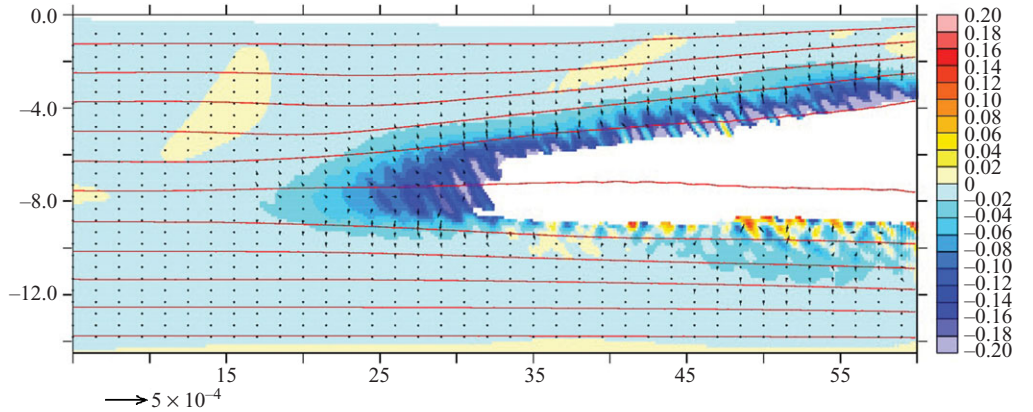

FIGURE 8. Cross-isopycnal variance flux component K_2 in $10^{-3}\,\mathrm{m^3\,s^{-3}}$ (shaded) and the flux ∇K_2 (arrows) which was also box-averaged. The vector shown below the figure corresponds to to $5 \times 10^{-4}\,\mathrm{m^2\,s^{-3}}$. K_2 was calculated setting $\theta_2 = 0$. Regions in which $|\nabla\bar{b}|^{1/2} < 0.015\,\mathrm{s^{-1}}$ are not shaded. Also shown are contours of the mean buoyancy (red lines).

Only in the region $20\,m \lesssim x \lesssim 30\,m$ the rotational variance flux shows a significant vertical (cross-isopycnal) component. In that region the rotational flux of variance makes up in fact a large portion of the 'total' cross-isopycnal flux of variance. Figure 8 shows K_2 (estimated again momentarily using $\theta_2 = 0$) which describes the diapycnal component of the 'total' flux of variance in the simulation. It is predominantly negative, i.e. the 'total' variance flux is directed up the gradient of mean buoyancy. In consequence, the rotational flux is reducing most of the impact of the effect of the diapycnal flux of variance in the Osborn–Cox relations (5.3) and (6.4). That means that the original Osborn–Cox relation, in which the advective fluxes of variance have been neglected is a surprisingly good approximation to the full TRM-G version of the Osborn–Cox relation (6.4) for this model configuration.

7. Approximate Osborn–Cox relations

The first term on the right hand side of (6.4) corresponds to the original Osborn–Cox relation (4.2)), while the remainder shows some resemblance with an expansion of an exponential function, although it is an operator. Formally, we might therefore interpret the series as an expansion of an operator $\mathscr{E}()$:

$$K_1 + \kappa = \kappa\overline{\mathscr{E}(b', \bar{b})}. \tag{7.1}$$

The analytical form of the operator $\mathscr{E}()$ remains unknown to us, but the first term of an expansion of $\mathscr{E}()$ would be identical to the original Osborn–Cox relation (4.2) which means that a first-order truncation to $\mathscr{E}()$ is given by $\mathscr{E}(b', \bar{b}) \approx 1 + C$.

However, we can come closer to the unknown operator $\mathscr{E}$ using the following slightly different expression for the budget of the buoyancy moments. We split the operator $\mathscr{D}$ in (6.4) into two components, i.e. $\mathscr{D} = D + \mathscr{F}$ with $D = \frac{\nabla^2\bar{b}}{|\nabla\bar{b}|^2}$ denoting an inverse $\bar{b}$ scale related to the curvature of the mean isopycnals. It is then possible to absorb the components related to the operator $\mathscr{F}$ (including the term $2\kappa\mathscr{F}\phi_n$ in (6.3)) by the rotational flux as outlined in the Appendix. However, we have to stress that this procedure can lead to an unphysical rotational eddy flux across the boundaries and that the definition of the rotational flux becomes ill-posed for the case of closed

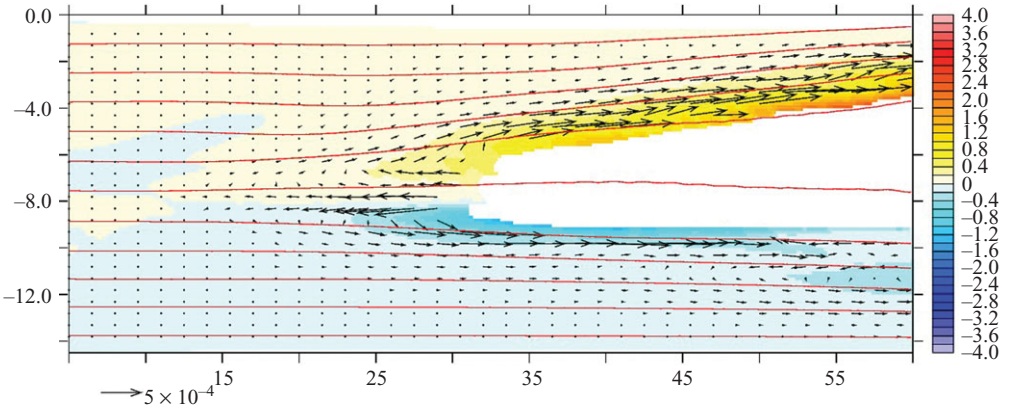

FIGURE 9. Approximative additional rotational flux potential $\chi_1 = \int \frac{\partial K_2}{\partial z}\, \mathrm{d}x$ in $10^{-3}\,\mathrm{m^3\,s^{-3}}$ (shaded) and resulting rotational flux (arrows). K_2 was calculated setting $\theta_2 = 0$. The flux vector was box averaged (12 points in x and 4 points in z direction). The vector shown below the figure corresponds to $5 \times 10^{-4}\,\mathrm{m^2\,s^{-3}}$. Regions in which $|\nabla\bar{b}|^{1/2} < 0.015\,\mathrm{s^{-1}}$ are not shaded. Also shown are contours of the mean buoyancy (red lines).

isopycnals. This artifact will be demonstrated with the aid of the numerical simulation below, although its effect on the turbulent diffusivity appears to be small.

Using the modified rotational flux $n\theta_n = B_{n+1} + \chi_n$ where the additional rotational gauge potential χ_n is given by the condition $\overline{\nabla\chi_n \cdot \nabla\bar{b}} = \overline{\nabla(K_{n+1} - 2n\kappa\bar{\phi}_n) \cdot \nabla\bar{b}}$ (see also the Appendix) the steady hierarchy of buoyancy moments becomes

$$K_1 = \kappa\overline{C} - DK_2, \quad K_n = \kappa(n-1)\overline{\phi_{n-1}(1+C)} - \frac{1}{n}DK_{n+1}. \tag{7.2}$$

Equation (7.2) no longer contains an operator, i.e. the operator $\mathscr{D}$ in (6.3) has been turned into the inverse buoyancy curvature scale D and the operator $\mathscr{F}$ was absorbed by rotational fluxes. Thus solving for K_1 in (7.2) and summing up is straightforward and yields an exact expression for the turbulent diffusivity

$$K_1 + \kappa = \kappa\overline{(1+C)\mathrm{e}^{-Db'}}, \tag{7.3}$$

in terms of the Cox number C and the dimensionless ratio Db' relating the tracer perturbation with the mean curvature scale D. We note that with the redefined rotational fluxes, the operator $\mathscr{E}$ can be expressed in analytical form as $\mathscr{E}(b', \bar{b}) = (1 + C)\mathrm{e}^{-Db'}$. For $D \to 0$ we recover the first-order approximation of the operator $\mathscr{E}$ and thus the original Osborn–Cox relation (4.2).

Figure 8 also shows the flux ∇K_2. Note that for $n = 1$ in (1) of the Appendix, the flux ∇K_2 together with the isopycnal flux of variance ∇B_2 and the molecular flux of variance has to be balanced by the redefined rotational flux $\nabla\theta_1$. It is clear that ∇K_2 is much smaller than the part related to the isopycnal flux of variance ∇B_2 (note that figures 6 and 8 show the fluxes using the same arrow scaling) such that the redefinition of θ_1 does not appear to have large consequences.

As defined in the Appendix, the cross-isopycnal projection of the flux ∇K_2 is meant to be balanced by the cross-isopycnal projection of the rotational flux $\nabla\chi_1$. The streamfunction for the rotational flux component χ_1 is shown in an approximate form as $\chi_1 = \int \frac{\partial K_2}{\partial z}\, \mathrm{d}x$ in figure 9, where the integration along isopycnals was replaced by an integration along z levels and the cross-isopycnal derivative by the vertical derivative

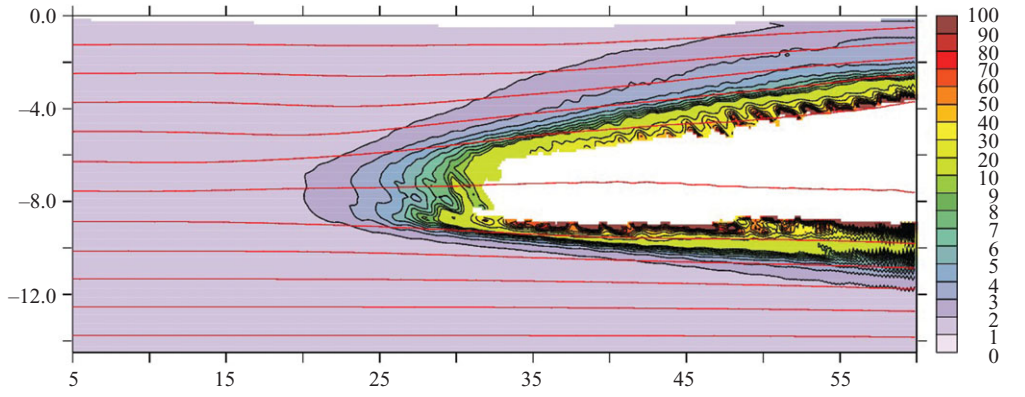

FIGURE 10. The modified Cox number $\overline{(1+C)\,\mathrm{e}^{-Db'}}$. Regions in which $|\nabla\bar{b}|^{1/2} < 0.015\,\mathrm{s}^{-1}$ are not shaded. Also shown are contours of the mean buoyancy (red lines).

for simplicity. The resulting rotational flux component $\overline{\nabla\chi_1}$ is also shown in figure 9 (again using the same arrow scaling as in figure 8). As outlined in the Appendix, the definition of χ_n is ill-posed in case of closed integration pathways. However, since we show here only a subset of the integration domain, we can formally apply this procedure in our simulation. The rotational eddy flux component $\overline{\nabla\chi_1}$ is of similar magnitude as $\overline{\nabla B_2}$, but its cross-isopycnal component is very small, in particular in the region $15\,\mathrm{m} \lesssim x \lesssim 30\,\mathrm{m}$ where we found large cross-isopycnal rotational fluxes. We might therefore expect that the redefinition of the rotational fluxes will not affect much the turbulent diffusivity K_1 in our model simulation.

On the other hand, the approximate rotational flux $\overline{\nabla\chi_1}$ shows a cross boundary flux, i.e. large positive fluxes at $x = 60\,\mathrm{m}$. Note the other part of the rotational flux, given by $\overline{\nabla B_2}$, recirculates within the domain, since the variance and thus the isopycnal projection of the variance flux is rapidly decaying in the restoring zone (which is not shown in the figures). However, there is no such recirculation for the flux related to χ_1, leading to an unphysical rotational flux across the right-hand side of our figure.

However, as long as the impact of the revised rotational flux remains small, which appears to be the case for our numerical simulation, we might regard the form (7.3) as a valid approximation to the operator $\mathscr{E}$ beyond the first-order approximation given by the original Osborn–Cox relation (4.2). The modified Cox number $\overline{(1+C)\mathrm{e}^{-Db'}}$ is shown in figure 10. It is in fact almost identical to the original Cox number $1+\bar{C}$. This is because for $D \to 0$, i.e. for strong mixing both numbers become identical. Therefore, we found again evidence that the original Osborn–Cox relation is a surprisingly good approximation to the generalized form Eq. (6.4).

8. Non-local estimates of diffusivity

In this section, we compare the above discussed estimated diffusivity and Cox numbers based on the Osborn–Cox relation with other interpretations and ways to estimate the turbulent diffusivity. Figure 11(*a*) shows the Cox number $K_{wd}/\kappa + 1$ related to the turbulent diapycnal diffusivity K_{wd} as given by the method by Winters & D'Asaro (1995). K_{wd} was derived from (7) and (12) of Winters & D'Asaro (1995) for which the instantaneous buoyancy b and the squared gradient of the instantaneous buoyancy $|\nabla b|^2$ are interpolated on the new tracer-dependent vertical coordinate z^*, which is given by (13) of Winters & D'Asaro (1995). The resulting

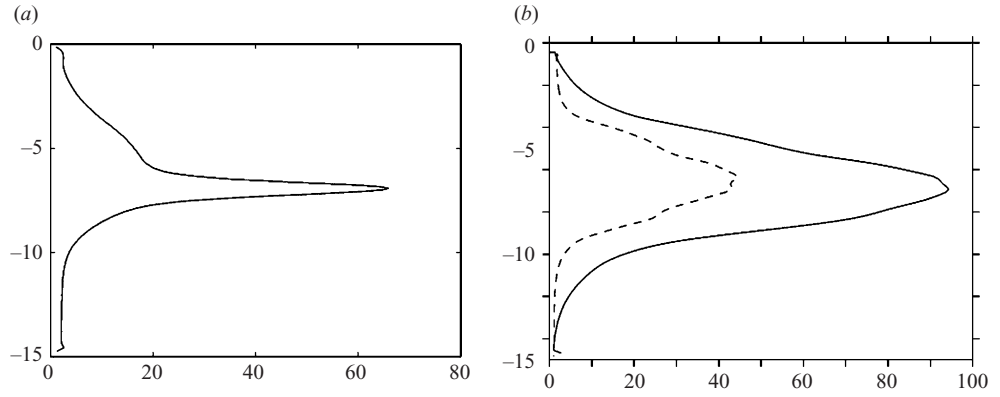

FIGURE 11. (a) The Cox number $K_{wd}/\kappa + 1$ related to the diapycnal diffusivity of Winters & D'Asaro (1995), K_{wd} as a function of z^* in metre (see text for definition). (b) $K_{TEM}/\kappa + 1$ (solid) and $1 + \bar{C}$ (dashed) as a function of z averaged along x in the entire channel.

$K_{wd}(t, z^*) = \kappa(\frac{db}{dz^*})^{-2} \langle |\nabla b|^2 \rangle$, where the brackets denote a spatial average at constant z^*, was also averaged over time and shown in figure 11 as a function of z^*. Note that the tracer-dependent coordinate z^* coincide with z for the case of horizontally undulated isopycnals and that $-15\,\mathrm{m} <= z^* <= 0\,\mathrm{m}$. It was shown by Winters & D'Asaro (1995) that K_{wd} is related to the total diapycnal irreversible flux across instantaneous isopycnals caused by the subgrid-scale diffusive mixing.

It was also shown by Winters & D'Asaro (1995) that K_{wd} is given by the subgrid-scale diffusivity κ times the ratio of the length of an instantaneous isopycnal compared to the length of the mean isopycnal. Note that K_{wd} is very similar to the effective diffusivity of Nakamura (1996) and that both approaches, due to their one-dimensional nature, are unaffected by spurious rotational fluxes.

Figure 11(a) shows that $K_{wd}/\kappa + 1$ is largest for $z^* \approx 7.5\,\mathrm{m}$ with values exceeding 60 but still much larger than one within the region $-10\,\mathrm{m} \lesssim z^* \lesssim -5\,\mathrm{m}$ indicating strong diapycnal mixing in this region as well. For comparison, figure 11(b) shows the previously discussed TEM-based mixing estimate (figure 3) as a function of z and averaged in x along the entire domain of the model. The TEM-based estimate of the diffusivity is much larger, while the estimate based on the Osborn–Cox relation, also shown in figure 11(b), is much smaller, i.e. comparable to the non-local estimates, demonstrating again the effect of the large rotational eddy fluxes in the TEM-based mixing estimate.

It should be noted, however, that the different diffusivities in figure 11 should be compared with care: The non-local diffusivity estimate of Winters & D'Asaro (1995), K_{wd}, is shown in figure 11(a) as a function of the tracer dependent coordinate z^*. In contrast, figure 11(b) shows the local diffusivity estimates using the classical Osborn–Cox relation and the TEM-based estimate averaged at constant depth z. The appearance of two different vertical coordinates, z^* and z, makes it difficult to compare the different estimates for the diffusivity directly. Furthermore, note that we average across the region of high turbulent mixing and low or vanishing stratification in the centre of the domain. Errors due to the low or vanishing stratification for the estimate using the original Osborn–Cox relation and the TEM framework are thus getting large. The Winters and D'Asaro method, on the other hand, is not effected by these errors. It becomes obvious that if one is interested in the diffusivity related to

basin averaged irreversible density flux and the corresponding diffusivity one should refer to K_{wd}. On the other hand, if one would like to consider spatial variations in diffusivity one should use the generalized Osborn–Cox relation to which the classical Osborn–Cox relation appears to be a reasonable first-order approximation in our model simulation.

9. Summary and discussion

In the TRM-G framework of Eden *et al.* (2007), the advective variance fluxes along mean isopycnals are interpreted as rotational eddy fluxes with no effect in the mean buoyancy budget and which should thus not be associated with a diapycnal diffusivity. It is only the genuinely diapycnal component of the variance fluxes which should be associated with a diapycnal diffusivity. In TRM-G, this diapycnal variance flux can be expressed as molecular (subgrid-scale) dissipation of buoyancy moments.

In the original Osborn–Cox relation (4.2), which is often used to estimate diapycnal diffusivity from observation estimates of molecular variance dissipation, all advective variance fluxes (and molecular fluxes, which should be small) are simply neglected. We assess the validity of this assumption and compare the results of the original Osborn–Cox relation in terms of estimates of diapycnal diffusivity with a generalized Osborn–Cox relation given by the TRM-G framework (defined in (6.4)), which yields a physically well motivated diapycnal diffusivity.

For this comparison, we used a numerical simulation of vertical shear instability with strong lateral inhomogeneity in turbulent mixing and with strong advective fluxes of variance. We found that advective fluxes of variance are indeed to a large extent associated with strong rotational eddy fluxes in the simulation. Relating those rotational eddy fluxes to a diapycnal diffusivity in a flux-gradient relation leads to a large overestimation of the diffusivity. In the generalized Osborn–Cox relation, the rotational eddy flux of tracer is used to cancel out the isopycnal flux of variance in the variance budget. We also found that much of the flux of variance, including the remaining cross-isopycnal flux of variance in the Osborn–Cox relation, is also of rotational nature which should also not be associated with the diapycnal diffusivity. This notion leads to the consideration of the complete hierarchy of buoyancy moments in the TRM-G which ultimately takes into account of all advective and molecular flux terms in the generalized Osborn–Cox relation leaving only dissipative terms associated with irreversible mixing of buoyancy to determine the diffusivity.

In our model simulation, the original Osborn–Cox relation holds to a surprisingly good approximation, despite the strong advective fluxes of variance and the large lateral inhomogeneity of turbulent mixing in the setup. This is because the advective and molecular fluxes of variance are cancelled out to a large extent by rotational eddy fluxes, which should not be associated with irreversible mixing of buoyancy. Although we cannot give a proof based on this single numerical experiment, we speculate that this result points towards a better applicability of the assumptions in the original Osborn–Cox relation, i.e. the neglection of advective and molecular fluxes, than one might have expected.

On the other hand, shear instabilities might generate less mixing in three dimensions than in our two-dimensional simulation, because secondary instabilities tend to flatten the overturning Kelvin–Helmholtz billows and reduce their mixing power. It might well be that in three dimensions the relative contribution of advection of variance and rotational eddy fluxes in the variance budgets become more important than

the dissipative contributions related to irreversible mixing of density, such that the original Osborn–Cox model might become less accurate as a first-order approximation to the generalized Osborn–Cox relation. Nevertheless, the mathematical framework developed here carries directly over to three dimensions leading to an expression for the diffusivity analogous to that in (6.4) (compare also Eden *et al.* (2007)).

The generalized Osborn–Cox relation is given by an infinite series of buoyancy moments, which can be interpreted as an expansion of an operator whose closed analytical form remain unknown to us. The first-order term of this expansion is given by the original Osborn–Cox relation. By modifying the definition of rotational fluxes in the TRM-G framework, we have formulated a closed analytical form of the Osborn–Cox operator given by (7.3), which approximates the full form given by (6.4), and which we found in the model simulation to be very similar to the results obtained using the original Osborn–Cox relation. A caveat of the procedure is, however, that it cannot be applied to cases with closed isopycnals. This is because it is necessary to allow for rotational fluxes across the boundaries where the mean isopycnals intersect. These rotational fluxes are needed to compensate for molecular fluxes and advective fluxes related to spatial variations of the turbulent diffusivity. However, given the simplicity of the closed analytical form, we argue that it represents a practical alternative to the full form of the generalized Osborn–Cox relation.

A drawback of the TRM-G framework and the (generalized) Osborn–Cox relation is that it involves higher order derivatives (or, for the case of the approximate form (7.3), an exponential function of buoyancy perturbations) which are difficult to estimate with enough accuracy from observations or from numerical model results. The approaches by Winters & D'Asaro (1995) and Nakamura (1996) overcome this difficulty by concentrating on the bulk effect of irreversible mixing related to subgrid-scale (molecular) processes. On the other hand, these approaches give by construction no information about the localization of the enhanced turbulent mixing in horizontal direction. Although it is clear that in our numerical experiment there is a large inhomogeneity in turbulent mixing in the horizontal direction, and thus also a large inhomogeneity in the turbulent diffusivity, the non-local approaches by Winters & D'Asaro (1995) and Nakamura (1996) to determine this diffusivity cannot show this inhomogeneity. In contrast, the TRM-G framework and the (generalized) Osborn–Cox relation do show this inhomogeneity but is in turn hampered by the higher order derivatives involved, which complicates the application, in particular in regions of weak stratification. The application of the different approaches therefore depends on whether or not a local estimate of the mixing is required.

This study was supported by the German DFG as part of the SFB 754. We thank three anonymous reviewers and the editor for their help to improve previous versions of this study.

Appendix

Using the flux decomposition (6.2) for $\boldsymbol{f}_n$ we rewrite the budget of the buoyancy moments (6.1) as

$$(\overline{\phi_{n+1}})_t + n\bar{\phi}_n\bar{b}_t + (n\underline{\nabla}\theta_n - \underline{\nabla}B_{n+1} + 2n\kappa\nabla\overline{\phi_n} - \nabla K_{n+1})\cdot\nabla\bar{b} = -n\kappa(n-1)\overline{\phi_{n-1}(|\nabla b'|^2 + |\nabla\bar{b}|^2)} + nK_n|\nabla\bar{b}|^2 + K_{n+1}\nabla^2\bar{b}, \quad (1)$$

(with $(n-1)\phi_{n-1}=1$ for $n=1$). With the setting $n\theta_n = B_{n+1}+\chi_n$ where the additional rotational potential χ_n is given by the condition $\overline{\nabla\chi_n\cdot\nabla\bar{b}} = \overline{\nabla(K_{n+1}-2n\kappa\overline{\phi_n})\cdot\nabla\bar{b}}$ all flux terms can be eliminated from the budget of buoyancy moments. Using this redefined rotational flux the steady hierarchy becomes (7.2). The potential χ_n can be obtained by integration along an isopycnal, since

$$\frac{\partial\chi_n}{\partial s} = \frac{\partial}{\partial n}(K_{n+1}-2n\kappa\overline{\phi_n}) \quad\rightarrow\quad \chi_n = \int \mathrm{d}s\left(\frac{\partial}{\partial n}(K_{n+1}-2n\kappa\overline{\phi_n}\right), \tag{2}$$

with the along-isopycnal derivative $\frac{\partial}{\partial s} = |\nabla\bar{b}|^{-1}\nabla\bar{b}\cdot\nabla()$ and the diapycnal derivative $\frac{\partial}{\partial n} = |\nabla\bar{b}|^{-1}\nabla\bar{b}\cdot\nabla()$. For the case of closed isopycnals, it is clear that the definition for χ_n is only possible if $\oint \frac{\partial}{\partial n}(K_{n+1}-2n\kappa\bar{\phi}_n)\,\mathrm{d}s = 0$ which is in general not the case. In the case of a period channel, contours of mean buoyancy are closed going from one end to the other, showing the limitation of this approach. However, using the redefined rotational flux it is possible to evaluate the diffusivity K_1 for the steady state

$$K_1+\kappa = \kappa\left[(1+\overline{C})-D\overline{\phi_1(1+C)}+D^2\overline{\phi_2(1+C)}-\frac{D^3}{2}\overline{\phi_3(1+C)}+\frac{D^4}{3!}\overline{\phi_4(1+C)}-\cdots\right]$$

Summing up yields an exact expression for the turbulent diffusivity K_1 given by (7.3).

REFERENCES

Andrews, D. G. & McIntyre, M. E. 1976 Planetary waves in horizontal and vertical shear: the generalized Eliassen–Palm relation and the zonal mean accelaration. *J. Atmos. Sci.* **33**, 2031–2048.

Andrews, D. G. & McIntyre, M. E. 1978 Generalized Eliassen–Palm and Charney–Drazin theorems for waves on axisymmetric mean flows in compressible atmosphere. *J. Atmos. Sci.* **35**, 175–185.

De Szoeke, R. A. & Bennett, A. F. 1993 Microstructure fluxes across density surfaces. *J. Phys. Oceanogr.* **23**, 2254–2264.

Dillon, T. M. & Park, M. M. 1987 The available potential energy of overturns as an indicator of mixing in the seasonal thermocline. *J. Geophys. Res.* **92** (C5) 5345–5353.

Eden, C., Greatbatch, R. J. & Olbers, D. 2007 Interpreting eddy fluxes. *J. Phys. Oceanogr.* **37**, 1282–1296.

Gregg, M. C. 1998 Estimation and geography of diapycnal mixing in the stratified ocean. In *Physical Processes in Lakes and Oceans* (ed. J. Imberger), Coastal and Estuarine Studies, vol. 54, pp. 305–338. Am. Geophys. Union.

McDougall, T. J. & McIntosh, P. C. 1996 The temporal-residual-mean velocity. Part I. Derivation and the scalar conservation equation. *J. Phys. Oceanogr.* **26**, 2653–2665.

McDougall, T. J. & McIntosh, P. C. 2001 The temporal-residual-mean velocity. Part II. Isopycnal interpretation and the tracer and momentum equations. *J. Phys. Oceanogr.* **31** (5), 1222–1246.

Medvedev, A. S. & Greatbatch, R. J. 2004 On advection and diffusion in the mesosphere and lower thermosphere: the role of rotational fluxes. *J. Geophys. Res.* **109** (D07104, 10.1029/2003JD003931).

Nakamura, N. 1996 Two-dimensional mixing, edge formation, and permeability diagnosed in an area coordinate. *J. Atmos. Sci.* **53**, 1524–1537.

Osborn, T. R. & Cox, C. S. 1972 Oceanic fine structure. *Geophys. Astrophys. Fluid Dyn.* **3** (1), 321–345.

Plumb, R. A. 1990 A nonacceleration theorem for transient quasi-geostrophic eddies on a three-dimensional time-mean flow. *J. Atmos. Sci.* **47** (15), 1825–1836.

Plumb, R. A & Ferrari, R. 2005 Transformed Eulerian-mean theory. Part I. Nonquasigeostrophic theory for eddies on a zonal-mean flow. *J. Phys. Oceanogr.* **35** (2), 165–174.

Schmitt, R. W., Ledwell, J. R., Montgomery, E. T., Polzin, K. L. & Toole, J. M. 2005 Enhanced diapycnal mixing by salt fingers in the thermocline of the tropical Atlantic. *Science* **308** (5722), 685–688.

Thorpe, S. A. 1977 Turbulence and mixing in a Scottish loch. *Phil. Trans. R. Soc. Lond. Ser.* A, *Math. Phys. Sci.* **286** (1334), 125–181.

Winters, K. B. & D'Asaro, E. A. 1995 Diascalar flux and the rate of fluid mixing. *J. Fluid. Mech.* **317**, 179–193.

Wunsch, C. & Ferrari, R. 2004 Vertical mixing, energy and the general circulation of the oceans. *Annu. Rev. Fluid Mech.* **36**, 281–314.